ROYAL SOCIETY OF CHEMISTRY

PAPER

Transparent nanocellulose hybrid films functionalized with ZnO nanostructures for UV-blocking†

Yaoquan Jiang,[a] Yuanyuan Song,[b] Miao Miao,[a] Shaomei Cao,[a] Xin Feng,*[ab] Jianhui Fang[c] and Liyi Shi[a]

Transparent, nanocellulose–ZnO (NC–ZnO) hybrid films were fabricated *via* a pressure controlled extrusion process using NC fibrils and sheet-like ZnO (s-ZnO) or belt-like ZnO (b-ZnO) nanostructures. The s-ZnO and b-ZnO conjoined with the NC fibrils to form a heterogeneous, fibrous network structure. The NC–ZnO hybrid films with different amounts of ZnO nanostructures showed a synergic feature of high optical transparency and excellent UV-blocking. The results indicated that NC assembled with s-ZnO hybrid film possessed excellent UV-blocking ability in a wide range from 200 to 375 nm, in contrast to NC–b-ZnO. Moreover, the prominent thermal and photo stability of transparent NC–ZnO hybrid films enhanced extensibility and ease of use for diverse biological applications, which require tolerance of temperature changes.

Introduction

With the decreasing stratospheric ozone content in the atmosphere, ultraviolet (UV) radiation from the solar spectrum is producing striking and ubiquitous detrimental effects on human health and other biological systems.[1–4] Excessive exposure to sunlight increases biological damage and degradation of organic compounds by UVA (320–400 nm) and UVB (280–320 nm) radiation.[5–7] Therefore, there is a need for the development of new generation self-protective sunscreen products such as visually transparent UV filters or coatings for UV-sensitive materials and lenses. Because petroleum-based polymer matrices cannot usually endure high temperatures,[8] a woven fabric essentially made from cotton or sisal fibers has become the primary means of protection in daily life. Unfortunately, UV radiation can easily penetrate ordinary woven fabrics.[9] Wang *et al.* prepared dumbbell-shaped ZnO with the aid of ZnO nanorods on the surface of cotton fabrics; the dumbbell-shaped ZnO presented a wider UV-blocking range (400–280 nm) than the ZnO nanosols (352–280 nm), ZnO nanorods (375–280 nm), and anatase titania films (332–280 nm).[10] Mao *et al.* covered cotton fabrics with needle-shaped ZnO nanorods; the nano ZnO-coated cotton fabrics have UV transmission in the UVB region (315–250 nm) and a part of the UVA region (370–315 nm).[11] Recently, Li *et al.* developed an effective route for fabricating hierarchical flower-like ZnO on cotton cellulose fibers by combining electrospinning with a low-temperature growth technique. The results indicated that cotton cellulose coated with flower-like ZnO has high absorption at a wavelength of 350 nm.[12] Wang *et al.* coated cotton textiles with ZnO@SiO$_2$ nanorods and found that the UV transmittance was significantly decreased. They believed that the excellent UV-blocking of the modified cotton textile could be ascribed to good absorption and strong scattering by the ZnO@SiO$_2$ nanorods array.[13] Due to its high strength, large surface area and unique optical properties, nanocellulose (NC) extracted from diverse native sources, including cotton, wood, bamboo, sisal, algae and bacteria, has received considerable attention in the last few decades.[14,15] NC-based films with firm and uniform networks have excellent optical transparency due to their nanometric fiber diameters; the light scattering is so decreased that a large part of the light transmits with no scattering. Furthermore, the transparent NC films with low coefficients of thermal expansion (12–28.5 ppm K^{-1}) are easier to process at high temperatures than plastic substrates.[16] The functionalized NC based films are of great interest when combined with exciting synergetic characteristics, including high transparency, outstanding biodegradability and excellent UV-blocking; they can be widely used for many applications, such as outdoor UV-sensitive polymers, car windshields, clean windows, contact lenses, and some special biological test containers.[17] As a typical II–VI semiconductor, ZnO exhibits a large exaction-binding energy (60 meV) and a wide band gap (3.37 eV).[18,19] It has attracted

[a] *Research Center of Nano Science and Technology, Shanghai University, Shanghai 200444, P. R. China. E-mail: fengxin@shu.edu.cn; Fax: +86 21 66136038; Tel: +86 21 66137257*

[b] *School of Materials Sciences and Engineering, Shanghai University, Shanghai 200444, P. R. China*

[c] *Department of Chemistry, Shanghai University, Shanghai 200444, P. R. China*

† Electronic supplementary information (ESI) available: SEM images of the cross-section of hybrid films, solid diffuse reflection UV-vis spectra, UV-vis spectra and photo-degradation results. See DOI: 10.1039/c5tc00812c

This journal is © The Royal Society of Chemistry 2015

J. Mater. Chem. C, 2015, **3**, 6717–6724 | 6717

tremendous interest owing to its remarkable environmentally friendly nature and chemical stability under exposure to both high temperatures and UV radiation.[20,21] ZnO nanostructures with large surface area to volume ratios have an increased UV-blocking effectiveness compared with that of bulk ZnO.[20]

All the studies mentioned above have demonstrated that woven fabrics combined with different ZnO nanostructures are beneficial in preventing UV radiation exposure. To date, great efforts have been devoted to the development of synthetic methodologies for ZnO nanostructures due to their promising applications.[22–26] NC is an ideal building block to host a range of guest ZnO nanomaterials to create UV protective transparent films for coating UV-sensitive substrates. However, the major issues that need to be addressed for the assembly of NC hybrid films with heterogeneous network architectures still remain. The main difficulty is extremely slow dewatering because of the high water binding capacity of NC;[27] conventional methods, such as suspension-casting, water evaporation, and hot pressing, used for removing the excessive water are extremely time-consuming, which require few days to several hours or even longer with complicated manipulations.[28]

Herein, highly transparent NC–ZnO hybrid films for UV blocking were rapidly assembled *via* a pressure extrusion dewatering method under ambient temperature using readily available starting materials. Different ZnO nanostructures were combined with a NC skeleton network to form heterogeneous fibrous hybrid films that exhibit synergic effects from ZnO and NC. The as-prepared hybrid films were characterized by XRD, FE-SEM, TG and UV-vis spectroscopy. By changing the amount of ZnO in the transparent NC based matrices, the UV-blocking abilities were preliminarily evaluated.

Experimental

Materials

All the reagents were of analytical grade and were used without any further purification. Zinc acetate dihydrate, anhydrous ethanol, urea, sodium hydroxide, hydrogen peroxide, sodium silicate, trisodium phosphate, Triton X-100, acetic acid, polyvinyl pyrrolidone, nitric acid and glycerol were purchased from Sinopharm Chemical Reagent Co., Ltd (Shanghai, China). Sodium chlorite was obtained from Aladdin Industrial Inc. (Shanghai, China).

Preparation of nanocellulose (NC)

Bamboo fibers were mechanically smashed to pass through a 200-mesh screen, followed by washing with distilled water. 160 g dried bamboo fibers, 2000 g distilled water and 60 g NaOH were first added to a three-necked, round-bottomed flask and heated at 100 °C for 2 h, then filtered and washed with distilled water to neutral pH. Second, the base-treated bamboo fibers were heated in 2000 mL distilled water, 1 wt% NaOH, 0.4 wt% Na_3PO_4 and 0.4 wt% (8 g) Na_2SiO_3 solutions (2000 mL) at 115 °C for 2 h, then filtered and washed with distilled water to neutral pH. Third, the delignified fibers were treated with

3.5 wt% NaOH, 0.7 wt% $NaClO_2$ and 150 mL CH_3COOH aqueous solutions (2000 mL) at 100 °C for 2 h, followed by 0.5 wt% Triton X-100 and 5 wt% aqueous solutions of citric acid (2000 mL) at 70 °C for 4 h, followed by washing with distilled water. Subsequently, bleaching was enhanced by continuing the reaction in aqueous solutions of 30 wt% H_2O_2 and 65 wt% HNO_3 (2 : 1 v : v) at 70 °C for 1 h, which was then filtered and washed thoroughly to neutral pH. The chemically treated aggregates were defibrillated according to a homogenization process with a high pressure homogenizer (D-3L, PhD Technology LLC, USA) for 3 cycles at a pressure of 5000 psi to obtain NC suspensions.

Preparation of sheet-like ZnO (s-ZnO)

Sheet-like ZnO was synthesized according to a modified literature method.[29] 2.16 g $Zn(OAc)_2·2H_2O$ was mixed with 1.90 g urea dissolved in 50 mL H_2O and transferred to a Teflon autoclave, then a $5 × 5$ cm^2 piece of cotton fabric was immersed into the solution. After the autoclave was heated at 140 °C for 24 h, the as-prepared precursor, collected from the cotton fabric, was calcined at 350 °C for 5 h to obtain s-ZnO.

Preparation of belt-like ZnO (b-ZnO)

Belt-like ZnO was prepared *via* a modified literature procedure;[30] 3.63 g $Zn(OAc)_2·2H_2O$, 6.43 g NaOH, 1.05 g PVP, 40 mL H_2O_2 and 400 mL distilled water were introduced into a Teflon autoclave and heated at 140 °C for 12 h. The sediment was washed with distilled water twice and dried at 70 °C to obtain ZnO_2. Subsequently, ZnO_2 was added to hydrazine hydrate (85%) with vigorous stirring, and then the resultant solution was transferred to a Teflon autoclave and heated at 150 °C for 24 h. Finally, b-ZnO was collected after washing and drying at 70 °C for 4 h.

Fast assembly of NC–ZnO hybrid films

NC–ZnO hybrid films were rapidly assembled as illustrated using an extrusion method.[31,32] 1.03 g NC suspension (2.93 wt%) was first diluted in 100 mL H_2O. Then, 100 mL diluted NC solution and a certain quantity of s-ZnO or b-ZnO and 0.50 g glycerol were mixed and sonicated with a high frequency ultrasonic cell disruptor (High Nova instrument Co., Ltd, China) at 700 W for 5 min to make a homogeneous solution. The as-prepared uniform dispersion was poured into the extruder (NanoAble-150, PhD Technology LLC, USA) to squeeze out the excess water under 2.0 MPa of N_2 gas. Subsequently, a gel cake emerged on the filter membrane (PC, Nuclepore Track-Etch Membrane, pore size 200 nm, Whatman, UK), which was peeled off, sandwiched between two glass plates and thoroughly dried at 95 °C for 10 min in a vacuum oven (0.1 MPa). NC–ZnO hybrid films doped with different amounts of ZnO were labeled as NC–s-ZnO$_x$ and NC–b-ZnO$_x$ (x = 0, 1, 2, 3, 4, 5, and 6 wt%). Transparent hybrid films 30 μm in thickness and 45 mm in diameter were ultimately prepared.

Characterization

The morphologies of the NC were observed with transmission electron microscopy (TEM) (JEM-200CX, JEOL, Japan) at an accelerating voltage of 120 kV. The morphologies of s-ZnO,

6718 | *J. Mater. Chem. C*, 2015, **3**, 6717–6724

This journal is © The Royal Society of Chemistry 2015

b-ZnO and hybrid films were investigated using a field emission scanning electron microscope (FE-SEM) (JSM-6700F, JEOL, Japan). The phase structures of the hybrid films were characterized using powder X-ray diffraction (XRD), which was carried out on a D/MAX2200 X-ray diffractometer equipped with Cu Kα1 (λ = 1.5418 Å) radiation operating at 40 kV and 40 mA. Diffuse reflectance UV-visible spectra were obtained using a UV-vis (2501PC, SHIMADZU, Japan) diode array spectrophotometer for dry-pressed disk samples, which were prepared by mixing ZnO and $BaSO_4$, and its scan range was 200–800 nm. The UV-blocking properties of the hybrid films were investigated by measuring their absorbance and transmittance with a UV-vis (2501PC, SHIMADZU, Japan) spectrophotometer. A Thermo Nicolet 6700 spectrometer (Thermo Fisher Scientific, USA) was used to record FT-IR spectra in transmission mode, ranging from 4000 to 400 cm^{-1}, using pressed KBr tablets prepared from finely ground samples mixed with dry KBr powder. The thermal stability of the hybrid films was studied using a NETZSCH STA409PC (Simultaneous Thermal Analyzer) instrument. The samples were analyzed at a heating rate of 10 °C min^{-1} in the range of 30–700 °C under air and N_2 atmosphere.

Results and discussion

Fig. 1 shows the TEM images of NC obtained before and after the homogenization process. As shown in Fig. 1a and b, the as-prepared NC has a uniform diameter distribution and conjoins to form a network structure. The dimensions of NC fibers range from 30 to 50 nm in width and 1–6 μm in length before the homogenization process. The impact of homogenization could break the relatively weak interfaces between the fibers, which are bonded mainly by van der Waals forces, resulting in overall decentralization of the NC fibers. It can be observed from Fig. 1b that the diameter of NC fibers after homogenization becomes 10–30 nm; meanwhile, the length decreases to 1–2 μm, which may assist the formation of transparent NC films.[33,34] SEM micrographs of s-ZnO and b-ZnO nanostructures are shown in Fig. 2. It is obvious that s-ZnO mainly consists of closely-packed monolayers, ~60 nm in thickness, and the synthetic b-ZnO consists of uniformly distributed nanobelts. The lengths of the nanobelts are typically tens of micrometers, the average width is 300 nm and the average thickness is about 100 nm.
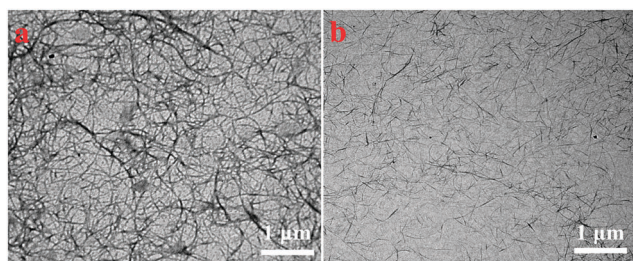

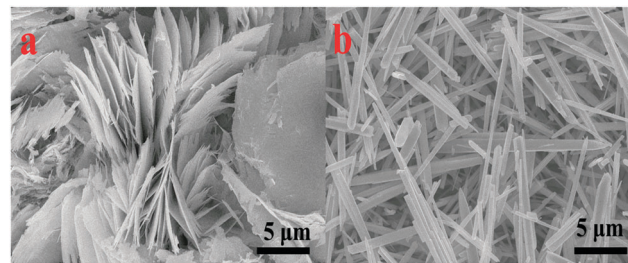Fig. 1 TEM images of NC (a) before and (b) after homogenization.

Fig. 2 SEM images of (a) s-ZnO and (b) b-ZnO nanostructures.

Digital images of NC–ZnO hybrid films and the relative SEM images of the surface morphologies of the hybrid films are presented in Fig. 3. It can be clearly seen that the NC films without the addition of ZnO nanostructures display high optical transparency, indicating that the films consist of cellulose fibers with nanometric diameters. The optical transparency of the hybrid films was maintained by adding appropriate amounts of ZnO nanostructures, indicating that ZnO combined uniformly with NC; this was beneficial to decrease the light scattering of NC–ZnO hybrid films. However, the transmittance of the hybrid films decreased as the stoichiometric ratio of ZnO immobilized into the NC fibrous network increased; these results were verified by the school emblem of Shanghai University under the hybrid films becoming more obscure. NC–b-ZnO$_x$ (x = 0, 1, 2, 3, 4, 5, and 6 wt%) hybrid films exhibit the most distinct characteristics and tendencies compared to NC–s-ZnO$_x$ (x = 0, 1, 2, 3, 4, 5, and 6 wt%), as shown in the left-hand columns of Fig. 3a and b. The right-hand columns of Fig. 3a and b illustrate the surface morphologies of NC–s-ZnO$_x$ hybrid films and NC–b-ZnO$_x$ hybrid films, respectively. It can be observed that the surfaces of the NC films are considerably smooth, but the flatness decreases with the addition of ZnO nanostructures.

The whiter sheet-like (Fig. 3a) or fibrillar (Fig. 3b) materials are ZnO nanostructures, which are well dispersed and embedded on the network of hybrid films without aggregation. The NC fibrous network acts as a template, allowing the high dispersity of ZnO nanostructures in the aqueous dispersion; thus, the individual ZnO nanostructures could adsorb stably on the NC fibrils by entangling with each other. It can be concluded that the high degree of transparency of the hybrid films can be ascribed to the high dispersity of ZnO nanostructures on the NC fibrous network. After increasing the additive amount of ZnO from 1 wt% to 6 wt%, a lot of ZnO nanostructures were gradually exposed on the surface of the hybrid films. It can also be seen from the SEM image that plenty of protruding spots, which are NC fibrils, were uniformly dispersed on the cross-section of pure NC film (Fig. S1a, ESI†). Moreover, the cross-sectional SEM images of hybrid films (Fig. S1b and c, ESI†) represented well-stacked structures without the aggregation of ZnO nanostructures. Moreover, the trace of s-ZnO drawn from the cross-section and the presence of b-ZnO embedded on the cross-section were obviously discerned. Consequently, the resulting microstructures and uniform distribution of ZnO nanostructures might be beneficial to the remarkable UV-blocking of the hybrid films.
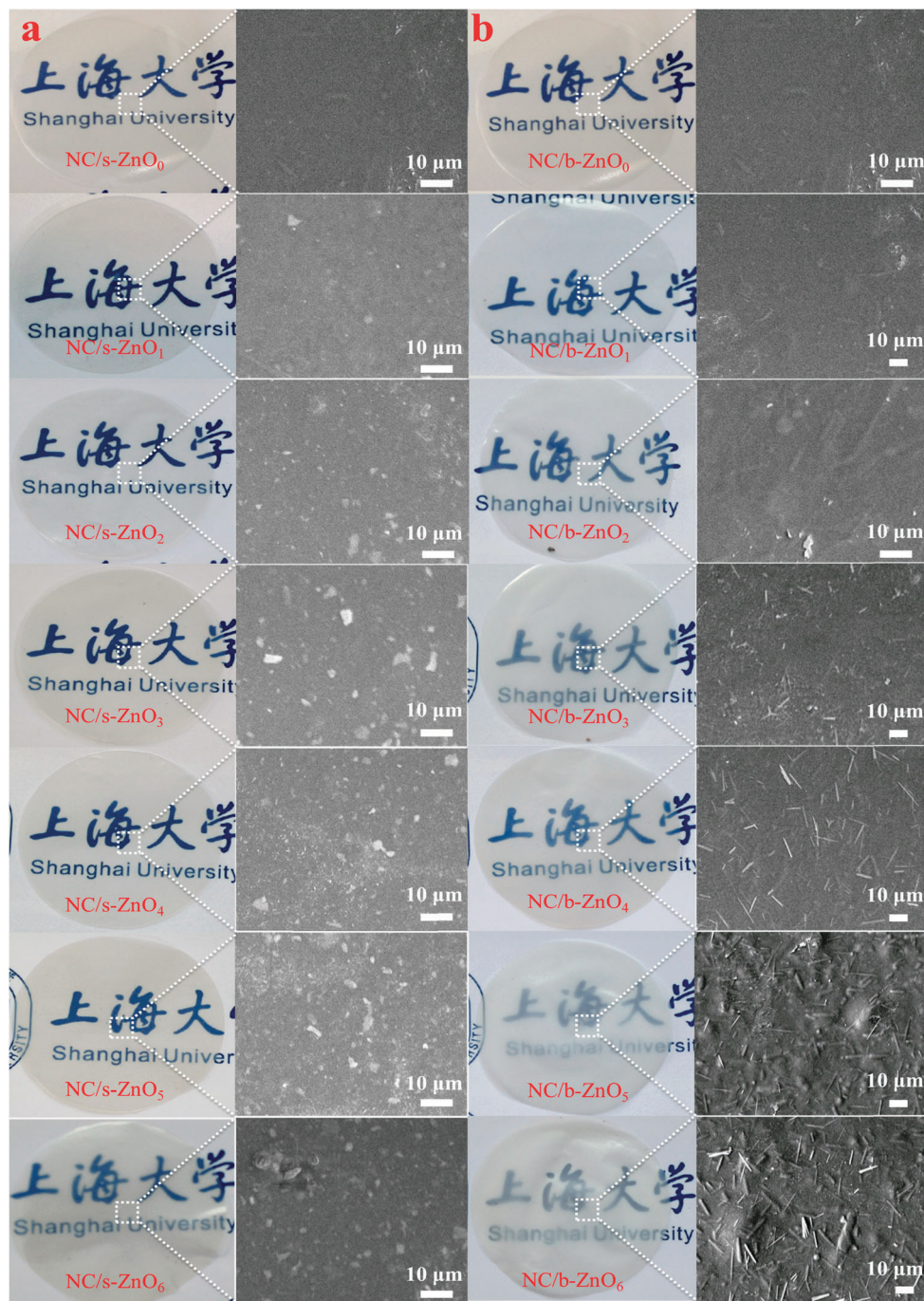
This journal is © The Royal Society of Chemistry 2015

J. Mater. Chem. C, 2015, 3, 6717–6724 | 6719

Fig. 3 Digital images and the relative SEM images of NC–ZnO$_x$ hybrid films, where x = 0, 1, 2, 3, 4, 5 and 6 wt%. (a) s-ZnO and (b) b-ZnO.

UV-vis spectra were recorded for the NC–ZnO hybrid films with different amounts of ZnO nanostructures by measuring the transmission.[35] The absorbance of NC–ZnO$_x$ (x = 0, 1, 2, 3, 4, 5, and 6 wt%) hybrid films can be seen in Fig. 4a and b, which show their UV-blocking ability. It is obvious that sharp and weak absorption peaks increase in intensity with increasing amounts of s-ZnO and b-ZnO, respectively. The UV absorption band of NC–s-ZnO hybrid films almost covers the whole UV range up to 400 nm. Moreover, Fig. 4c and d show the optical transmittance plotted against the wavelength for

NC–ZnO$_x$ (x = 0, 1, 2, 3, 4, 5, and 6 wt%) hybrid films with different ZnO nanostructures. It can be clearly seen that NC–s-ZnO hybrid films have excellent UV-blocking performance, superior than that of NC–b-ZnO hybrid films. However, as the content of ZnO nanostructure increases, the transmittance decreases dramatically. The neat NC films have high optical transparency and some UV blocking ability. However, by incorporating ZnO nanostructures into NC matrices, UV photons with wavelengths in the range from 200 to 375 nm are efficiently absorbed by the NC–s-ZnO hybrid films. Moreover, a
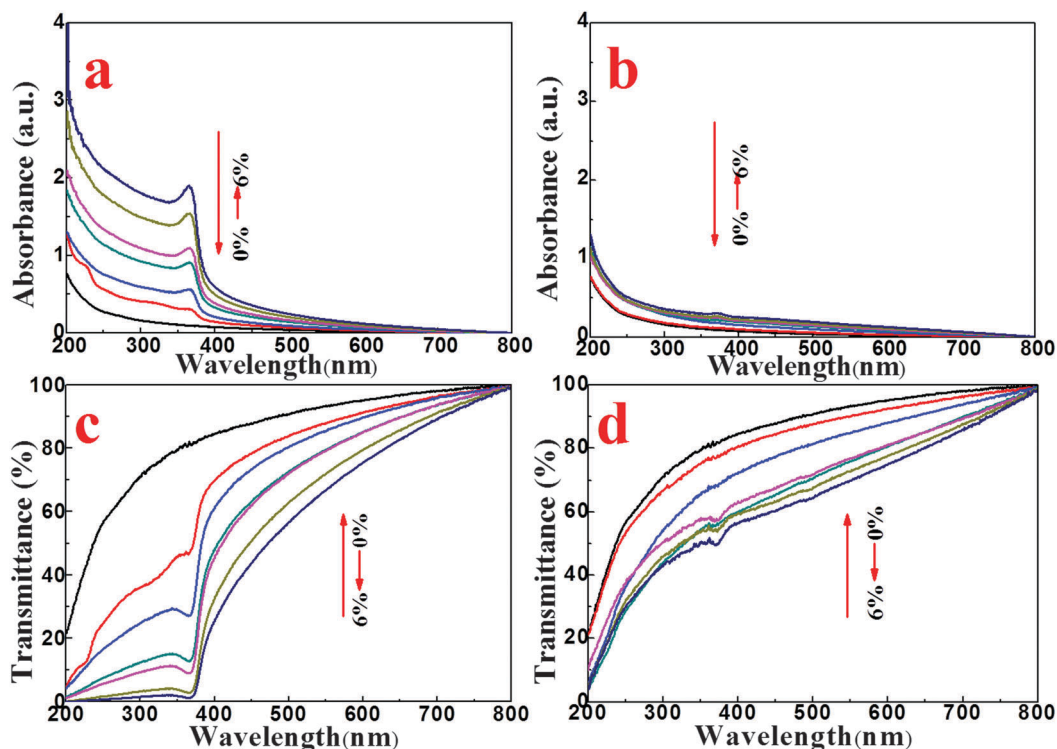
6720 | *J. Mater. Chem. C*, 2015, **3**, 6717–6724

This journal is © The Royal Society of Chemistry 2015

Fig. 4 UV-vis spectra of NC−s-ZnO$_x$ (a, c) and NC−b-ZnO$_x$ (b, d) hybrid films with different amounts of ZnO (x = 0, 1, 2, 3, 4, 5, and 6 wt%).

high amount of s-ZnO results in enhanced UV-blocking efficiency over 90% of the UV region. The results indicated that s-ZnO had better size and dimension effects compared to b-ZnO, thereby enhancing the UV-blocking efficiency.[36] Nanocomposites possessing both high visible light transparency and high UV light resistance are desirable for a range of important applications.[26,36,37] The transmittance, the visible-shielding ratio (VR) and the UV-blocking ratio (UVR) of NC–ZnO hybrid films are shown in Table 1. Herein, T(%)-s550 and T(%)-b550 are the transmittances of NC–s-ZnO and NC–b-ZnO hybrid films at 550 nm. UVR-s300 and UVR-b300 are the UVRs of NC–s-ZnO and NC–b-ZnO hybrid films at 300 nm. UVR-s225 and UVR-b225 are the UVRs of NC–s-ZnO and NC–b-ZnO hybrid films at 225 nm. The transmittances of NC–s-ZnO hybrid films are similar to those of NC–b-ZnO hybrid films at 550 nm. Eqn (1) was used to evaluate the VR and UVR at 300 nm, 225 nm and 550 nm of the films.[9]

$$R(\%) = (T_0 - T)/T_0 \qquad (1)$$

where T_0 is the transmittance of as-prepared pure NC films and T is the transmittance of the films. The UVR increases with increasing wt% of ZnO nanostructures, indicating that the UVRs of NC–s-ZnO hybrid films at 300 nm and 225 nm are higher than those of NC–b-ZnO hybrid films up to 97.79% and 99.13%, respectively. The solid diffuse reflection UV-vis spectra (Fig. S2, ESI†) further verified that s-ZnO possessed better UV reflection compared to b-ZnO, which corresponded to the evidence that NC–s-ZnO hybrid films had a higher UVR. The VRs of NC–s-ZnO and NC–b-ZnO hybrid films at 550 nm were also evaluated. The results indicated that the VR increased with

Table 1 The transmittance, visible-shielding ratio (VR) and UV-blocking ratio (UVR) of NC−s-ZnO and NC−b-ZnO hybrid films

	NC–Zn	NC–ZnO$_1$	NC–ZnO$_2$	NC–ZnO$_3$	NC–ZnO$_4$	NC–ZnO$_5$	NC–ZnO$_6$
T(%)-s550	93.39	87.84	85.44	79.49	79.12	71.81	66.70
T(%)-b550	93.39	90.08	84.84	75.78	76.74	72.71	69.81
VR-s550	0	5.94	8.51	14.88	15.28	23.19	28.58
VR-b550	0	3.54	9.70	18.86	17.83	22.14	25.25
UVR-s300	0	49.28	65.17	82.56	86.87	95.37	97.79
UVR-b300	0	6.05	24.10	38.33	28.87	35.58	39.72
UVR-s225	0	70.98	74.88	89.56	91.82	97.98	99.13
UVR-b225	0	5.32	51.03	62.95	38.55	55.97	56.23

the ZnO content. Consequently, NC–s-ZnO hybrid films with s-ZnO contents of 3 wt% and 4 wt% exhibit high UV light absorption and low absorption of visible light and hence high UV-blocking efficiency and high visible light transparency. In addition, the optical properties of NC–s-ZnO hybrid films were investigated by bending them 200 times at an angle of 135°. It can be seen that the changes in transmittance and absorbance are negligible (Fig. S3, ESI†). Therefore, it can be reasonably foreseen that the UV-blocking ability of the as-obtained transparent NC–s-ZnO hybrid films will pave the way for a large variety of applications in human health and other biological systems.

Fig. 5 shows the XRD patterns of NC–s-ZnO$_x$ and NC–b-ZnO$_x$ hybrid films. The peaks at 14.7°, 16.5°, 22.7° and 35.0° can be indexed as the typical (101), (101), (200), and (040) reflections of cellulose I.[9,38] On increasing the addition of s-ZnO, the intensities of the ZnO characteristic peaks at 31.8°, 34.4°,
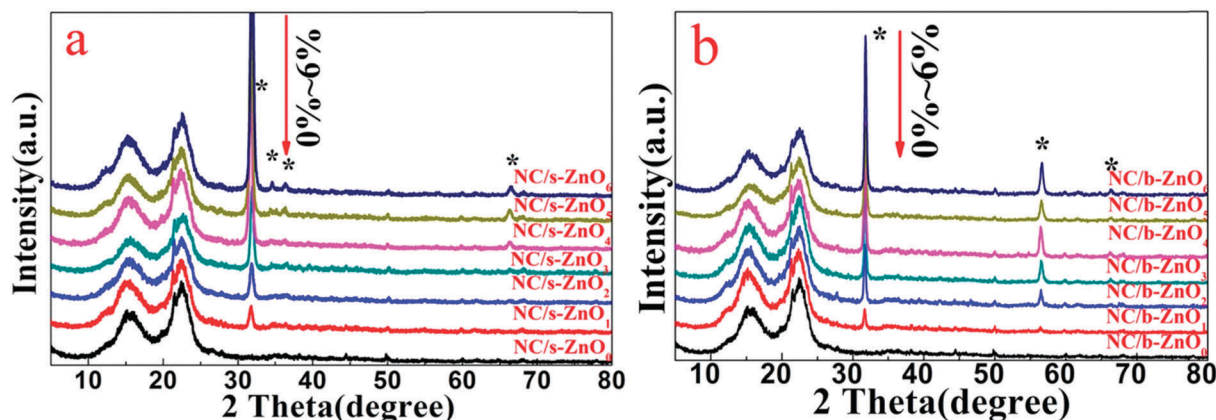
Fig. 5   XRD patterns of NC−s-ZnO$_x$ (a) and NC−b-ZnO$_x$ (b) hybrid films with different amounts of ZnO nanostructures (x = 0, 1, 2, 3, 4, 5, and 6 wt%).

36.4° and 66.2° gradually increase.[39] However, for NC–b-ZnO$_x$ hybrid films, there is a relatively stronger peak at 56.6° with the addition of b-ZnO (Fig. 5b), compared with the main peaks of NC–s-ZnO$_x$ hybrid films, as shown in Fig. 5a. Therefore, it can be deduced that the b-ZnO nanostructures have different crystalline structures and a very high c-axis growth-orientation. The results indicated that NC fibrils were successfully assembled with different ZnO nanostructures to form heterogeneous hybrid films.

The thermal stability of NC–ZnO hybrid films was an important factor for diverse applications that require tolerance of temperature changes. Fig. 6 clearly demonstrates the thermal degradation of the NC–ZnO hybrid films under air and N$_2$ atmosphere with different amounts of ZnO nanostructures. For comparative purposes, the TG curve of NC–s-ZnO$_0$ film under a N$_2$ atmosphere was also presented and correlated well with the reported literature.[40] The total weight loss of the NC film is 100 wt% after heating up to about 575 °C, and there is a 35 wt% weight loss at about 300 °C, which is attributed to the desorption of moisture. All the samples exhibited a significant weight loss at about 320 °C, which is ascribed to the decomposition of NC.[41] With the addition of ZnO$_x$ (x = 1, 3%), the TG

curves of hybrid films under a N$_2$ atmosphere are almost similar to that of NC film, but the thermal stability of NC–ZnO hybrid films increases. Under air atmosphere, another mass loss stage ranging from 350 °C to 470 °C could be observed. The second mass loss for the degradation of NC fibrils under oxidative atmosphere is commonly designated to the oxidation of charcoal formed by the primary pyrolysis reaction.[42] The weight under N$_2$ and air atmosphere still remains at about 1 wt% and 3 wt%, respectively, at a temperature of about 700 °C. This evidence further indicated that ZnO nanostructures were successfully embedded into the NC fibrils to form a heterogeneous network structure.
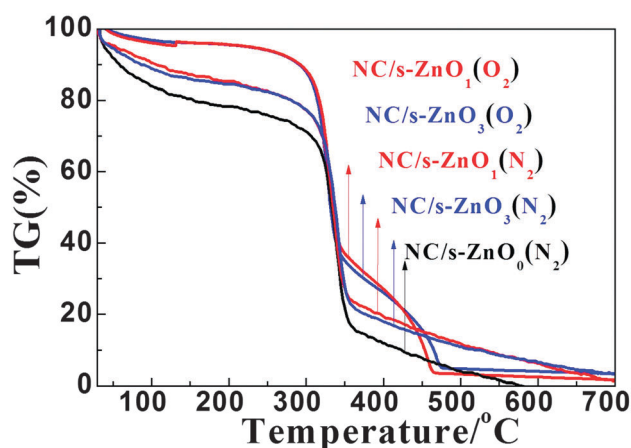

Fig. 6   TG curves of NC−s-ZnO hybrid films with different amounts of ZnO nanostructures of 0 wt%, 1 wt%, and 3 wt%.
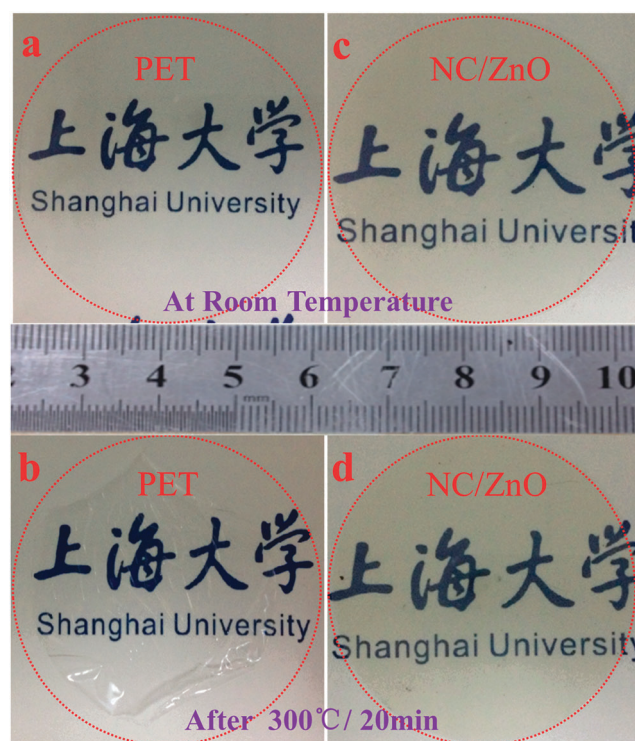

Fig. 7   Digital pictures of PET film (a, b) and NC−s-ZnO (c, d) film at room temperature and after heating at 300 °C for 20 min.

Fig. 7 compares the thermal stability of NC–s-ZnO hybrid film with that of PET film by measuring the dimensional change. After heating at 300 °C for 20 min, the PET film shows a large thermal shrinkage and wrinkle (Fig. 7b); however, the dimensional change of the NC–ZnO hybrid film is negligible (Fig. 7d). The outstanding thermal stability of NC–s-ZnO hybrid films was due to the anomalous characteristics of NC.[43] Another interesting observation from this study is that NC–ZnO hybrid films have perfect photo stability under UV irradiation for about 72 h (Table S1, ESI†). This is due to the superior UV light screening effect offered by the addition of ZnO nanostructures.

Conclusions

In summary, transparent NC–ZnO hybrid films were successfully fabricated *via* a pressure-controlled extrusion process using NC fibrils as a soft matrix and s-ZnO or b-ZnO nanostructures as functional fillers. The different ZnO nanostructures were uniformly dispersed in the NC network structure, as observed by SEM. NC–s-ZnO hybrid films thus exhibited more prominent UV-blocking properties than NC–b-ZnO hybrid films with the same amount of ZnO. The as-prepared NC–s-ZnO hybrid films with s-ZnO contents of 3 wt% and 4 wt% possessed both high transparency and excellent UV-blocking properties. The UV-blocking ratio of NC–s-ZnO hybrid films with an s-ZnO content of 6 wt% was 97.79% and 99.13% at 300 nm and 225 nm, respectively, which are much higher than those of NC–b-ZnO hybrid films. Therefore, we demonstrate herein a facile strategy to prepare transparent NC–ZnO hybrid films, which could be applied for the realization of transparent, low-cost, lightweight, and flexible substrates in UV-blocking fields.

Acknowledgements

Notes and references

1 J. B. Kerr1 and C. T. McElroy, *Science*, 1993, **262**, 1032.
2 M. Berneburg, H. Plettenberg and J. Krutmann, *et al.*, *Photodermatol., Photoimmunol. Photomed.*, 2000, **16**, 239.
3 M. R. Albert and K. G. Ostheimer, *J. Am. Acad. Dermatol.*, 2002, **47**, 930.
4 C. E. Williamson, P. J. Neale and G. Grad, *et al.*, *Ecol. Appl.*, 2001, **11**, 1843.
5 F. R. de Gruijl, *Eur. J. Cancer*, 1999, **35**, 2003.
6 H. Stege, L. Roza and A. A. Vink, *et al.*, *Proc. Natl. Acad. Sci. U. S. A.*, 2000, **97**, 1790.
7 H. Hattori, Y. Ide and T. Sano, *et al.*, *J. Mater. Chem. A*, 2014, **2**, 16381.
8 K. Q. Han and M. H. Yu, *J. Appl. Polym. Sci.*, 2006, **100**, 1588.
9 Y. Li, Y. L. Zou and Y. Y. Hou, *et al.*, *Cellulose*, 2011, **18**, 1643.
10 R. H. Wang, J. H. Xin and X. M. Tao, *et al.*, *Inorg. Chem.*, 2005, **44**, 3926.
11 Z. P. Mao, Q. P. Shi and L. P. Zhang, *et al.*, *Thin Solid Films*, 2009, **517**, 2681.
12 C. R. Li, Y. Xie and Q. Y. Liu, *et al.*, *Fibers Polym.*, 2014, **15**, 281.
13 L. L. Wang, X. T Zhang and B. Li, *et al.*, *ACS Appl. Mater. Interfaces*, 2011, **3**, 1277.
14 Y. Habibi, L. A. Lucia and O. J. Rojas, *et al.*, *Chem. Rev.*, 2010, **110**, 3479.
15 Q. Song, W. T. Winter and B. M. Bujanovic, *et al.*, *Energies*, 2014, **7**, 607.
16 J. Huang, H. G. Zhu and Y. C. Chen, *et al.*, *ACS Nano*, 2013, **7**, 2106.
17 T. Y. Wang, T. T. Isimjan and J. F. Chen, *et al.*, *Nanotechnology*, 2011, **22**, 265708.
18 X. Feng, J. P. Zhang and W. Shi, *et al.*, *Mater. Technol.*, 2010, **25**, 35.
19 X. Feng, L. Y. Shi and S. F. Wang, *et al.*, *Solid State Ionics*, 2008, **179**, 2077.
20 A. Becheri, M. Dürr and P. L. Nostro, *et al.*, *J. Nanopart. Res.*, 2008, **10**, 679.
21 Y. Tu, L. Zhou and Y. Z. Jin, *et al.*, *J. Mater. Chem.*, 2010, **20**, 1594.
22 Ü. Ö. Ya. I. Alivov and A. Liu, *et al.*, *J. Appl. Phys.*, 2005, **98**, 041301.
23 Z. J. Xing, B. Y. Geng and X. L. Li, *et al.*, *CrystEngComm*, 2011, **13**, 2137.
24 Y. B. He, G. R. Li and Z. L. Wang, *et al.*, *Energy Environ. Sci.*, 2011, **4**, 1288.
25 C. M. Chang, M. H. Hon and I. C. Leu, *et al.*, *Sens. Actuators, B*, 2010, **151**, 15.
26 Z. X. Wang, X. Y. Zhan and Y. J. Wang, *et al.*, *Nanoscale*, 2012, **4**, 2678.
27 M. Österberg, J. Vartiainen and J. Lucenius, *et al.*, *ACS Appl. Mater. Interfaces*, 2013, **5**, 4640.
28 M. Nogi, S. Iwamoto and A. N. Nakagaito, *et al.*, *Adv. Mater.*, 2009, **21**, 1595.
29 J. H. Pan, X. W. Zhang and J. D Alan, *et al.*, *Phys. Chem. Chem. Phys.*, 2012, **14**, 7481.
30 X. Cao, N. Wang and L. Wang, *et al.*, *J. Nanopart. Res.*, 2010, **12**, 143.
31 J. P. Zhao, Z. W. Wei and X. Feng, *et al.*, *ACS Appl. Mater. Interfaces*, 2014, **6**, 14945.
32 M. Miao, J. P. Zhao and X. Feng, *et al.*, *J. Mater. Chem. C*, 2015, **3**, 2511.
33 H. L. Zhu, S. Parvinian and C. Preston, *et al.*, *Nanoscale*, 2013, **5**, 3787.
34 H. Koga, T. Saito and T. Kitaoka, *et al.*, *Biomacromolecules*, 2013, **14**, 1160.

This journal is © The Royal Society of Chemistry 2015

J. Mater. Chem. C, 2015, **3**, 6717–6724 | **6723**

35 G. Y. Zhang, Y. Liu and H. Morikawa, *et al.*, *Cellulose*, 2013, **20**, 1877.

36 Y. Q. Li, S. Y. Fu and Y. W. Mai, *Polymer*, 2006, **47**, 2127.

37 Y. Ren, M. Chen and Y. Zhang, *et al.*, *Langmuir*, 2010, **26**, 11391.

38 Q. L. Lu, W. Y. Lin and L. R. Tang, *et al.*, *J. Mater. Sci.*, 2015, **50**, 611.

39 A. Kumar, H. Gullapalli and K. Balakrishnan, *et al.*, *Small*, 2011, **7**, 2173.

40 G. G. Alves, P. A. A. P. Marques and C. P. Neto, *et al.*, *Cryst. Growth Des.*, 2009, **9**, 386.

41 C. Katepetch, R. Rujiravanit and H. Tamura, *et al.*, *Cellulose*, 2013, **20**, 1275.

42 D. K. Shen, J. M. Ye and R. Xiao, *et al.*, *Carbohydr. Polym.*, 2013, **98**, 514.

43 S.-J. Chun, E.-S. Choi and E.-H. Lee, *et al.*, *J. Mater. Chem.*, 2012, **22**, 16618.